THE ASTROPHYSICAL JOURNAL, 564:327–332, 2002 January 1

HIGH-RESOLUTION MID-INFRARED IMAGING OF G339.88−1.26

JAMES M. DE BUIZER,[1,2] ANDREW J. WALSH,[3] ROBERT K. PIÑA,[2,4] CHRIS J. PHILLIPS,[5] AND CHARLES M. TELESCO[2,4]

Received 2001 June 19; accepted 2001 September 10

ABSTRACT

G339.88−1.26 is considered to be a good candidate for a massive star with a circumstellar disk. This has been supported by the observations of linearly distributed methanol maser spots believed to delineate this disk and mid-infrared observations that have discovered a source at this location that is elongated at the same position angle as the methanol maser distribution. We used the mid-infrared imager/spectrometer OSCIR at Keck Observatory to make high-resolution images of G339.88−1.26. We resolve the mid-infrared emission into three sources within 1″.5 of the location of the masers. We determine that the methanol masers are most likely not located in a circumstellar disk. Furthermore, we find that the observed radio continuum emission most likely comes from two sources in close proximity to each other. One source is an unobscured massive star with an extended H II region that is responsible for the peak in the radio continuum emission. A second source is embedded and centered on the elongation in the radio continuum emission that is believed to be tracing an outflow in this region.

Subject headings: H II regions — infrared: ISM — ISM: individual (G339.88−1.26) — ISM: jets and outflows — masers — stars: formation

1. INTRODUCTION

It is generally accepted that stars form via accretion processes, and they achieve their final masses predominantly through accretion of star-building material from a circumstellar disk (for a review, see Boss 2000). It is from these accretion disks that planetary systems are thought to eventually form. Observations of accretion disks and accreting protostars have supported this hypothesis in the case of low- and solar-mass stars (Boss 2000). However, there has been no such observational support of the accretion disk scenario in the high-mass portion of the stellar mass spectrum. Some authors suspect that high-mass stars are created through a different process than low-mass stars, like low-mass protostellar mergers, for instance (for a review, see Garay and Lizano 1999).

On the other hand, circumstantial evidence of circumstellar disks around massive stars does exist in the form of radio wavelength emission from outflows and masers. Outflow is an important indirect indicator of the presence of a circumstellar disk. In the accretion paradigm, when the star is gaining mass via accretion from a disk, it is also accompanied by a bipolar outflow that is collimated by the disk. The presence of a disk may also be ascertained from observations of molecular masers. Maser emission from various molecular species has been observed for several decades and is a well-known indicator of recent massive star formation. These masers occur in spatially localized regions or "spots" and serve as probes of the small-scale structure, dynamics, and physical conditions of the environments near forming stars. Radio observations by Norris et al. (1998) and Phillips et al. (1998) have shown that methanol (CH_3OH) maser spots are frequently distributed in linear patterns, with projected dimensions typically spanning 2500 AU. Furthermore, in many cases the velocities of the individual maser spots show a linear trend across the source, indicative of the masers tracing a rotating structure. It has thus been plausibly argued that in these cases the methanol maser spots occur in, and directly delineate, rotating circumstellar disks. However, other authors (Sobolev & Deguchi 1994; Walsh et al. 1998) suggest that such linear arrangements of masers, and even their systemic velocities, may be explained by shock models.

G339.88−1.26 is one such site of linear methanol masers. It was observed to have ionized material elongated at a position angle perpendicular to the maser spot distribution angle by Ellingsen, Norris, & McCulloch (1996), who claim the masers are located within a disk. This hypothesis seems to have been reaffirmed by the first mid-infrared observations of this source by Stecklum & Kaufl (1998), which showed a 10 μm source elongated at the same position angle as the methanol masers. It was suggested that this was thermal emission from the dust in the circumstellar disk in which the methanol masers existed. However, independent mid-infrared observations in a survey by De Buizer, Piña, & Telesco (2000) showed that the source had more structure at 18 μm, resolving what appeared to be a companion source lying at the same position angle as the source elongation.

To date, G339.88−1.26 is considered to be one of the best candidates for being a massive star with a circumstellar accretion disk and to be good evidence that methanol masers exist in circumstellar disks. In this paper we present new high-resolution images of G339.88−1.26 taken from the Keck II telescope. The increased angular resolution reveals details not seen before in the mid-infrared and uncovers a region of a different nature than previously thought.

2. OBSERVATIONS AND DATA REDUCTION

Observations were obtained at Keck II between 11 and 13 hr UT on 1999 April 30 and again between 12 and 13 UT

[1] Cerro Tololo Inter-American Observatory, National Optical Astronomy Observatory, Casilla 603, La Serena, Chile. CTIO is operated by AURA, Inc., under contract to the National Science Foundation.
[2] Visiting Astronomer, W. M. Keck Observatory.
[3] Max-Planck-Institut für Radioastronomie, Auf dem Huegel 69, D-53121, Bonn, Germany.
[4] Department of Astronomy, 211 Space Sciences Research Building, University of Florida, Gainesville, FL 32601.
[5] Joint Institute for VLBI in Europe, Radiostrerrenwacht Dwingeloo, Postbus 2, 7990 AA Dwingeloo, The Netherlands.

on May 1. The University of Florida mid-infrared camera/spectrometer OSCIR was used for all observations. OSCIR employs a Rockwell 128 × 128 pixel Si:As BIB (blocked impurity band) detector, with a 0.″0616 pixel^{-1} scale at Keck II. The total field of view of the array is 8″ × 8″. Images were taken through two filters, $N(\lambda_o = 10.46\ \mu m, \Delta\lambda = 5.1\ \mu m)$ and IHW18($\lambda_o = 18.06\ \mu m, \Delta\lambda = 1.7\ \mu m$). Images were centered on a methanol maser reference feature at R.A. (J2000) = $16^h52^m04^s.66$, Decl. (J2000) = −46°08′34.″2. Keck II images presented in this paper are composites made up of several images (two for N, four for IHW18) with on-source exposure times of 120 s each, which were then registered and stacked to improve the signal-to-noise ratio. Background subtraction was achieved during observations via the standard chop-nod technique. Flux density calibration was achieved by observing at a similar airmass the mid-infrared standard star η Sgr, for which the flux densities were taken to be 188 Jy at N and 66 Jy at IHW18. Point-spread function (PSF) stars were also imaged near the position of G339.88−1.26, yielding a measured FWHM of 0.″33 at N and 0.″41 at IHW18. Because of time constraints, there was no attempt to perform accurate astrometry for the observations.

Using the 10 and 18 μm data, we constructed dust color temperature (T) and emission optical depth (τ) maps for each source. To do so, the 10 μm source image was convolved with an 18 μm PSF and the 18 μm source image with a 10 μm PSF so that both images are at exactly the same spatial resolution. Next we employed two techniques to find the best spatial registration of the two images. First we used an automated registration algorithm based on minimizing the sum of the squared residuals of the image difference as a function of the relative offsets. This algorithm generates a "χ^2" surface at integral x- and y-pixel offsets. The χ^2 surface may then be interpolated to determine the location of the minimum to fractional pixel values. The second method was to simply overlay the two images and acquire the best perceived registration visually. This alignment was a relatively easy task owing to the source brightnesses and similar structure seen at both wavelengths. Offsets found from these two techniques were in agreement to within 2 pixels. We therefore estimate the alignment between the 10 and 18 μm images to be accurate to better than 0.″1 (2 pixels).

Once the image set was spatially registered, the 10 and 18 μm flux densities for each pixel were used to iteratively solve for emission optical depth (τ) at 10 μm and dust color temperature. For these calculations we used the relationship $\tau_{10\ \mu m} = \tau_{18\ \mu m}/1.69$ (from the extinction law of Mathis 1990). Tests showed that shifts in alignment between the two convolved images within the above quoted 2 pixel error can change the peak temperature and optical depth values by ±7%. Furthermore, these shifts can create slight changes (<0.″2) in peak locations; however, the overall trends in the temperature and optical depth distributions are preserved.

3. RESULTS AND DISCUSSION

Presented in Figures 1*a* and 1*b* are the 10 and 18 μm images, respectively, from Keck II. These images show only the source referred to as G339.88−1.26:DPT00 1 from De Buizer et al. (2000). One can see that the simple elongated source first seen by Stecklum & Kaufl (1998) with the ESO 3.6 m telescope is now resolved into three mid-infrared components. The western source seen in these Keck II images, which we will refer to as G339.88−1.26:DPT00 1C, is the same as that resolved by De Buizer et al. (2000) on the Cerro Tololo Inter-American Observatory 4 m with OSCIR. However, the Keck II images show that there are two sources to the east of 1C.[6] The easternmost source is the brightest at 18 μm (G339.88−1.26:DPT00 1A), but the flux density peak at 10 μm is the source between 1A and 1C (G339.88−1.26:DPT00 1B). Finding integrated flux densities for these sources is difficult because they each display extended morphologies and are embedded in a region of more extended emission. The integrated flux densities tabulated in Table 1 are found by using a two-dimensional Gaussian model to subtract off one source in the pair and then performing aperture photometry on the second. Given this uncertainty, combined with atmospheric variability and uncertainty in the standard star flux density, we quote the flux density values for these sources in Table 1 with a 10% photometric error.

The eastern source 1A is elongated at a position angle of ∼315° (more clearly seen in the 18 μm image). The central source 1B may be extended, as seen in the 10 μm image (Fig. 1*a*); however, the surface brightness distribution in this source may be confused by the close proximity of 1A. Source 1C has a diffuse appearance, and the emission appears as if dust has been swept up to the northwest in a "tail," an effect seen predominantly in the 18 μm image.

3.1. *The Nature of the Sources*

The dust color temperature and optical depth maps are shown in Figure 1*c* and 1*d*, respectively. The temperature map shows that the temperature peak (∼145 K) is 0.″4 due west of the mid-infrared peak of source 1B and that the temperature drops off uniformly to the west and east. Clear temperature peaks, such as this one, indicate the positions of the stellar heating sources. The optical depth map shows that emitting material here is optically thin at 10 μm and that the optical depth is higher for 1A and 1C than for 1B.

Qualitatively, the mid-infrared surface brightness distribution of the sources appear similar to the observations of the circumstellar disk of HR 4796A (Jayawardhana et al. 1998; Koerner et al. 1998). Analogous to the mid-infrared observations of HR4796, G339.88−1.26 has three aligned mid-infrared sources with a temperature peak near the central mid-infrared source, delineating the stellar source. Likewise, the eastern and western sources in G339.88−1.26 can be thought of as being analogous to the lobes of a disk. However, the disk scenario seems unlikely for several

[6] We will use a shortened form of the IAU recommended names; i.e., G339.88−1.26:DPT00 1C will be referred to as 1C.

TABLE 1

MID-INFRARED PHOTOMETRY

Source	Flux Density (mJy) 10 μm Integrated	10 μm Peak	18 μm Integrated	18 μm Peak
1A	358 (± 36)	1.0 (± 0.1)	7964 (± 796)	13.0 (± 1.3)
1B	202 (± 20)	1.3 (± 0.1)	934 (± 93)	7.8 (± 0.8)
1C	99 (± 10)	0.6 (± 0.1)	3464 (± 346)	4.4 (± 0.4)

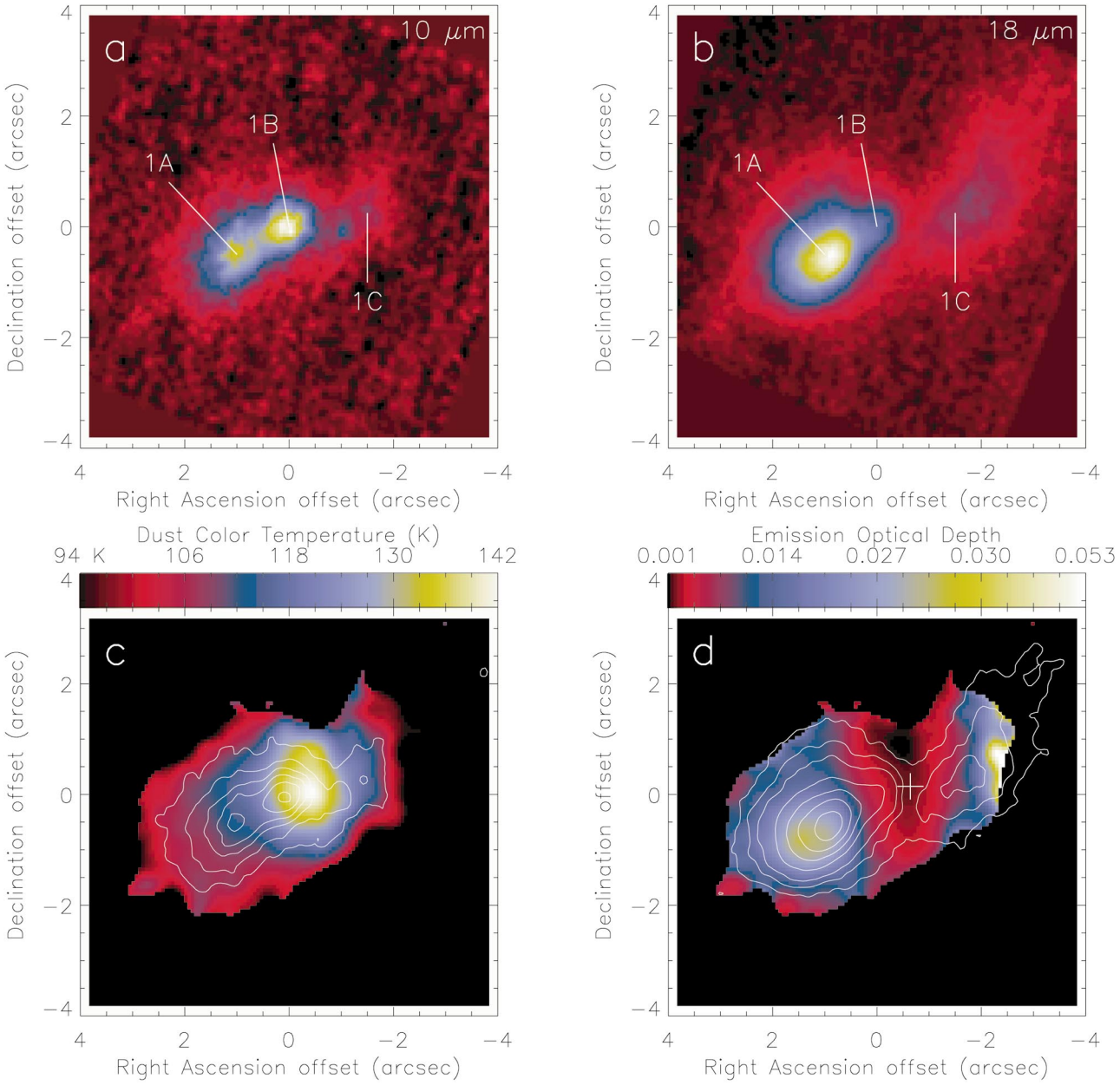

FIG. 1.—Color OSCIR images from Keck II at 10 μm (*a*) and 18 μm (*b*), resolve the source into three mid-infrared components labeled 1A, 1B, and 1C. The dust color temperature map (*c*) is overlaid with the 10 μm contours and shows that the temperature peak is 0.″4 west of source 1B. The emission optical depth map (*d*) is overlaid with the 18 μm contours. A cross marks the temperature peak location.

reasons. First, at 18 μm, sources 1A and 1C are significantly different in brightness, and it would be difficult in disk models to explain such a disparity in the flux densities on opposite sides of a circumstellar disk. Furthermore, the wispy, diffuse appearance of 1C is an unlikely morphology for a lobe of a disk, and it would be difficult to explain this tail of emission rising northward. Finally, the temperature peak is offset from the mid-infrared peak of 1B. As discussed in the section on observations and data reduction, shifts in the temperature peak can be caused by improper registration of the 10 and 18 μm convolved images. However, tests showed that there was no alignment of the two images within our estimated error that could produce a temperature peak at the location of the mid-infrared peak of source 1B, and the predominant change in temperature peak position (<0.″2) in these trials was in the north-south direction. Therefore, we are confident that the offset between the temperature peak and mid-infrared peak of 1B is real. Consequently, it seems unlikely that 1B is the circumstellar dust surrounding the stellar source present at this temperature peak.

So what is responsible for the temperature peak? There is a radio continuum source at the location of G339.88−1.26:DPT00 1, seen at 8.6 GHz by Ellingsen, Norris, & McCulloch (1996) and Walsh et al. (1998). Walsh et al. (1999) discovered a source at H (1.65 μm) and K (2.2 μm) that is coincident with the location of the radio continuum peak. Furthermore, this source seen in the near-infrared can also be seen in the Digitized Sky Survey at visible wavelengths. An important question to answer is does the optical/near-infrared source and the radio continuum source have the same origin? It is certainly plausible

from the fact that the optical, near-infrared, and radio sources are all coincident within their respective positional errors. However, the optical/near-infrared source may be photospheric emission from a foreground object, with the radio source coming from a second deeply embedded object. We can rule out a further possibility that there is only one deeply embedded object, because we can see the source optically.

We can use our mid-infrared observations to help clarify the situation. We see a temperature peak in Figure 1*c* indicating the presence of a source hotter than those sources seen in the mid-infrared. Therefore, the optical/near-infrared emission most likely originates from the location of the dust temperature peak. If this optical/near-infrared source is a foreground source, we surmise that it must be close enough to the dusty material we see in the mid-infrared to directly heat it. We do not see any evidence for a peak in either the 10 or 18 μm dust emission maps (Figs. 1*a* and 1*b*) at the position of the temperature peak, something we would assume from an embedded ultracompact H II region. Therefore, we have no evidence that there is a second embedded source at the same position as the optical/near-infrared source. Thus, we conclude that the most plausible scenario is that the optical, near-infrared, and radio continuum emission all come from a star located just in front of the mid-infrared sources.

At first glance, it appears contradictory that we find compact radio continuum emission around a star that can be seen in the optical. However, the radio continuum observations by Ellingsen et al. (1996; shown in Fig. 2) were made using the 6A configuration of the Australia Telescope Compact Array (ATCA), which is insensitive to large structures. Further observations, using a more compact configuration of the ATCA (S. Ellingsen 2001, private communication), show resolved emission extending over approximately 30″. We estimate the spectral type of the star to be B2.5 on the basis of the integrated radio flux of 14 mJy and a distance of 3.1 kpc. The Strömgren radius of a B2.5 star is expected to be 0.3 pc, assuming an electron density of 10^{-4} cm^{-3}. At a distance of 3.1 kpc, this is equivalent to a diameter of 40″. Thus, the size of the ionized region agrees well with that expected from an unembedded H II region around a B2.5 star. Since the source responsible for this radio peak is also seen at wavelengths as short as visible, this star could not be significantly embedded in circumstellar material. In fact, the mid-infrared emission optical depth decreases to the lowest value at this location.

It therefore appears that there are four different sources in this small region: 1A, 1B, 1C, and the optical/near-infrared/radio continuum source, which is unobscured and located at the temperature peak. Although we have no information on the three-dimensional distribution of the sources in this region, the close two-dimensional proximity of the dusty source 1B to this unobscured stellar source indicate that it is perhaps slightly foreground to 1B. A possible scenario is that the optical/near-infrared/radio source formed from the same molecular cloud containing the other sources but is located on the edge closest to us.

In Figure 2*a*, we show radio continuum data from Ellingsen et al. (1996). From this map it is easy to see that the continuum is elongated and that there are also other knots in the radio map extending far beyond the compact center. Line cuts in the x-pixel direction were made through the map of the radio source to find the peak flux density along the source as a function of pixel position y. A linear regression line was fit to these points, yielding a position angle for

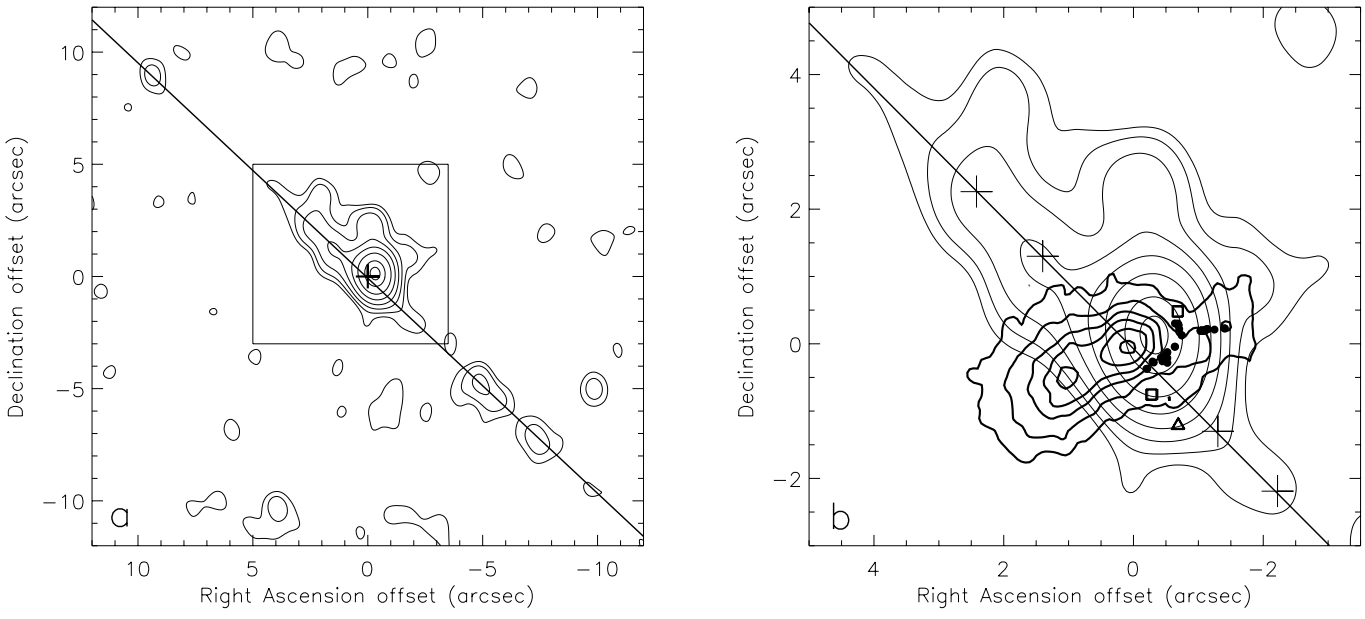

FIG. 2.—Radio continuum emission from G339.88−1.26. (*a*) A wide field of view contour map of the 8.59 GHz radio continuum data of Ellingsen et al. (1996). The emission around the radio continuum peak is elongated, and there are other knots of radio emission lying along the elongation axis (*diagonal line*). We suggest that this radio emission marks an ionized outflow. (*b*) The probable relationship between the radio and mid-infrared emission. The 10 μm thick contours are shown overlaid with the radio continuum contours (thin contours shown in the box in panel *a*), assuming the radio continuum peak is coincident with the optical/near-infrared stellar source at the location of the color temperature peak. Overplotted are the methanol masers (*filled circles*) from C. Phillips et al. (2002, in preparation), the water maser (*triangle*) from Forster & Caswell (1989), and the OH masers (*squares*) from Caswell, Vaile, & Forster (1995). The outflow axis does not intersect the radio continuum peak, but instead the mid-infrared peak of source 1B. The crosses mark the positions of two possible bipolar mass loss events that are equidistant from the location of 1B.

the elongation. The continuum around the radio peak was found to be elongated at a position angle of 46°, and it appears that the separate knots of radio continuum extend out in both directions along this axis. Given the collimated nature of the radio continuum, we suggest that it is likely to be tracing an ionized outflow. In Figure 2*b* we show the 10 μm contours, overlaid with the radio continuum contours centered on the dust temperature peak location. However, it can be seen in this figure that the collimated outflow axis does not bisect the radio peak but instead bisects the mid-infrared source 1B. Thus, it seems there are two components contributing to the radio continuum emission: an ionized outflow from 1B and a second component aligned with the temperature peak. This strengthens our astrometric argument that the radio continuum peak is located at the dust temperature peak. This is the only registration of the radio continuum peak that yields a source on the outflow axis.

We suggest that source 1B is an embedded protostar (since we see no temperature peak at its location) with an ionized outflow. Interestingly, the 10 μm image of 1B shows that it may be elongated at a position angle roughly perpendicular to the axis of outflow. This elongation may be due to a disk; however, we caution that it may also be due to slight differences in the positions of the individual frames that were stacked to make the final image and/or confusion of extended emission from source 1A. The possible elongation of 1B cannot be confirmed at 18 μm because of the confusion with source 1A. In Figure 2*b*, it can be seen that there are knots of radio continuum emission located equidistant from the location of 1B (*crosses*), which may have been bipolar mass loss events in the past. This again strengthens our astrometric argument that 1B is the center of the outflow and that the radio continuum peak is associated with the dust temperature peak (and thus, the optical/near-infrared source). The presence of ionized components of the outflow in such close proximity to the location of 1B implies that the protostar here is still actively outflowing. Assuming the outflowing material is moving at the speed of a standard high-velocity outflow of $\sim$20 km s^{-1} (Bachiller 1996), the age of the closest outflow event to 1B would be approximately 1300 yr, given a distance of 3.1 kpc (Walsh et al. 1997). However, ionized radio jets from massive stars have been observed with velocities a magnitude or more than this value (Rodriguez 1996), so these outflow events may have been much more recent. The central elongation of the radio continuum is more prominent to the northeast than to the southwest, perhaps owing to inclination effects, or perhaps owing to anisotropy in the parent molecular cloud; however, there are also some bright knots of ionized material seen along the outflow axis to the southwest.

In Figure 1*d*, we see that the eastern optical depth peak follows the 18 μm flux density contours of source 1A quite well. Since this source has a low-emission optical depth at 10 μm, and since there is no temperature peak at the location of 1A, it is likely that this source is bright in the mid-infrared simply because we are seeing through a large column of mid-infrared emitting material. This knot of material may be heated externally by either 1B or the optical/near-infrared stellar source.

This same scenario seems likely for 1C, as well. However, 1C is morphologically distinct in that it has a wispy, "coma"-like appearance. One cannot help but draw morphological similarities to mid-infrared observations of AFGL 2591 (Marengo et al. 2000). This site contains two sources, AFGL 2591A and AFGL 2951B, with the latter displaying a morphology similar to G339.88−1.26:DPT00 1C. One scenario given for the morphology of source AFGL 2951B is that it is a protostar whose envelope may be affected by an observed outflow from AFGL 2951A, creating the coma-like shape. In the same manner, it is a possibility that a less-collimated molecular component of the outflow coming from G339.88−1.26:DPT00 1B along the axis of the ionized component may be responsible for the morphology of G339.88−1.26:DPT00 1C.

3.2. *The Methanol Masers*

The relative astrometry between the radio continuum and methanol masers presented in Figure 2 is accurate to 0.″2 (C. Phillips et al. 2002, in preparation). The methanol masers plotted were observed using the Australian VLBI network (C. Phillips et al. 2002, in preparation). These observations are more sensitive to the weaker masers than the observations of Norris et al. (1993) and show 49 masers in the distribution. Because of the higher spatial resolution, the relative positions of the maser components are much more accurate and do not suffer from spatial or spectral blending. The majority of the methanol masers are strung along in a distribution that runs from the east and curves up to the north. There is also a western group of methanol masers that are linearly distributed in an east-west fashion.

What is it that the methanol masers are delineating? The string of masers (not including the western group) may be tracing a disk (as suggested by Norris et al. 1998) around the star at the center of 1B, but the masers in this string lie, on average, 0.″6 from the mid-infrared peak, given our astrometry. A necessary condition for masers to be in an edge-on disk is that they are coincident with the mid-infrared peak denoting the center of a circumstellar dust distribution. If our astrometry is correct, it would be unlikely that the methanol masers are located in an edge-on disk. This string of methanol masers tends to follow the radio continuum contours well. However, they just as likely could be said to appear to trace the outer mid-infrared contours of 1B. Therefore, a more likely explanation is that these methanol masers are tracing a shock or density enhancement, perhaps in the material around 1B.

The western group of methanol masers form a line that is coincident with the brightest part of source 1C. It is not clear how they may be excited. However, it is possible that they are shock induced as well by the outflow from 1B into the material of 1C.

4. CONCLUSIONS

We have resolved what was once thought to be a single circumstellar disk into three mid-infrared sources near the location of the methanol masers of G339.88−1.26. Furthermore, a reinspection of the radio continuum observations of Ellingsen et al. (1996) reveals a well-collimated distribution of radio sources, which we claim is due to an ionized outflow. This outflow axis does not bisect the radio continuum distribution peak, and it therefore seems likely that the source responsible for the ionized outflow is not the same source responsible for the radio continuum peak.

The true relative alignment between the radio and mid-infrared sources is unknown, and mid-infrared observations with more accurate astrometry are needed. However, using all of the available observations of G339.88−1.26 we have

found the most probable astrometric scenario. In this scenario it appears that this small region not only contains the three mid-infrared sources but also includes a non–mid-infrared emitting stellar source seen in the optical and near-infrared. It is coincident with the location of the radio continuum peak, and we therefore argue that this stellar source has an associated H II region and is probably a massive star of spectral type B2.5. We also find that the axis of the elongated radio continuum bisects the mid-infrared source 1B, which appears to lie at the center of, and be responsible for, the ionized outflow. Given our astrometry, the methanol masers appear offset from the peaks of the mid-infrared sources, and therefore it is most probable that the methanol masers are not tracing an edge-on disk in this case, as claimed by De Buizer et al. (2000), De Buizer (2000), and Ellingsen et al. (1996). A majority of the methanol masers seem to be associated with source 1B, although our astrometry places a grouping of methanol masers at the location of 1C. It is unclear exactly how the methanol masers in this region are excited; however, on the basis of purely morphological arguments for source 1B, we suggest a more probable supposition is that they lie in the surrounding dusty envelope.

The authors would like to thank Simon Ellingsen for the generous use of his radio data. Some of the data presented herein were obtained at the W. M. Keck Observatory, which is operated as a scientific partnership among the California Institute of Technology, the University of California, and NASA. The Observatory was made possible by the generous support of the W. M. Keck Foundation.

REFERENCES

Bachiller, R. 1996, ARA&A, 34, 111
Boss, A. P. 2000, in ASP Conf. Ser. 219, Disks, Planetesimals, and Planets, ed. F. Garzon et al. (San Fransico: ASP), 7
Caswell, J. L., Vaile, R. A., & Forster, J. R. 1995, MNRAS, 277, 210
De Buizer, J. M. 2000, in ASP Conf. Ser. 219, Disks, Planetesimals, and Planets, ed. F. Garzon et al. (San Fransico: ASP), 162
De Buizer, J. M., Piña, R. K., & Telesco, C. M. 2000, ApJS, 130, 437
Ellingsen, S. P., Norris, R. P., & McCulloch, P. M. 1996, MNRAS, 279, 101
Forster, J. R., & Caswell, J. L. 1989, A&A, 213, 339
Garay, G., & Lizano, S. 1999, PASP, 111, 1049
Jayawardhana, R., Fisher, S., Hartmann, L., Telesco, C., Pina, R., & Fazio, G. 1998, ApJ, 503, L79
Koerner, D. W., Ressler, M. E., Werner, M. W., & Backman, D. E. 1998, ApJ, 503, L83
Marengo, M., Jayawardhana, R., Fazio, G. G., Hoffmann, W. F., Hora, J. L., Dayal, A., & Deutsch, L. K. 2000, ApJ, 541, L63
Mathis, J. S. 1990, ARA&A, 28, 37
Norris, R. P., et al. 1998, ApJ, 508, 275
Norris, R. P., Whiteoak, J. B., Caswell, J. L., Wieringa, M. H., & Gough, R. G. 1993, ApJ, 412, 222
Phillips, C. J., Norris, R. P., Ellingsen, S. P., & McCulloch, P. M. 1998, MNRAS, 300, 1131
Rodriguez, L. F. 1996, Rev. Mexicana Astron. Astrofis., 4, 7
Sobolev, A. M., & Deguchi, S. 1994, A&A, 291, 569
Stecklum, B., & Kaufl, H. 1998, ESO Press Release PR 08/98
Walsh, A. J., Burton, M. G., Hyland, A. R., & Robinson, G. 1998, MNRAS, 301, 640
———. 1999, MNRAS, 309, 905
Walsh, A. J., Hyland, A. R., Robinson, G., & Burton, M. G. 1997, MNRAS, 291, 261